# A Maximum Efficiency Point Tracking Control Scheme for Wireless Power Transfer Systems Using Magnetic Resonant Coupling

Hongchang Li, *Student Member, IEEE*, Jie Li, Kangping Wang, *Student Member, IEEE*, Wenjie Chen, *Member, IEEE*, and Xu Yang, *Member, IEEE*

***Abstract*—With a good balance between power transfer distance and efficiency, wireless power transfer (WPT) using magnetic resonant coupling is preferred in many applications. Generally, WPT systems are desired to provide constant output voltage with the highest possible efficiency as power supplies. However, the highest efficiency is not achieved by the reported closed-loop WPT systems that maintain constant output voltage against coupling and load variations. In this paper, an efficiency evaluation method is put forward to evaluate the closed-loop control schemes. Furthermore, a maximum efficiency point tracking control scheme is proposed to maximize the system efficiency while regulating the output voltage. This control scheme is unique and prominent in that it fixes the operating frequency at the receiving-side resonant frequency and converts both the input voltage and the load resistance at the same time. Thus, the maximum efficiency point on the constant output voltage trajectory can be tracked dynamically. Therefore the system's output voltage can be maintained constant and its efficiency is always the highest. The experimental results show that the maximum efficiency point is tracked and a very high overall efficiency is achieved over wide ranges of coupling coefficient and load resistance.**

***Index Terms*—Closed-loop system, maximum efficiency point tracking (MEPT), voltage regulation, wireless power transfer (WPT).**

## I. Introduction

DELIVERING electrical power wirelessly has been desired since Tesla's principle of wireless transmission of energy [1], [2]. With a good balance between power transfer distance and efficiency, wireless power transfer (WPT) using magnetic resonant coupling is preferred in many daily and industrial applications [3], such as wireless chargers for smartphones [4], electric vehicles [5]–[7], and biomedical implants [8]–[11].

Generally, WPT systems are desired to provide constant output voltage with the highest possible efficiency as power supplies. However, the output voltage and the efficiency of an open-loop WPT system depend strongly on the coils' coupling coefficient and the system's load [12], [13]. Even worse, both the coupling coefficient and the load impedance are usually inconstant. For instance, in a wireless charging system for electrical vehicles, the coupling coefficient depends on customers' placement, and the load (battery) impedance also changes during charging. Therefore, there are two most important challenges in design and control of a WPT system. The first one is output voltage regulation. The second one is system efficiency maximization [14]. The motivation of this paper is to fulfill both of these two requests at the same time.

To provide a constant output voltage, an open-loop WPT system can be appropriately designed to make the output voltage insensitive to coupling or load variation [15]. However, a closed-loop control is necessary to maintain an accurate constant output voltage. The reported closed-loop regulation methods can be classified into three groups: frequency tracking, impedance matching, and dc/dc conversion. First, the constant voltage gain against coupling and load variations can be achieved by tracking the split frequencies in the "over coupled" region if the coupled resonances are lossless [9], [11], [16]. Moreover, a power-level tracking method that adaptively adjusts the operating frequency with output power feedback is put forward in [17]. Second, the dynamic impedance matching circuits switched by relays or semiconductor switches are mentioned to maximize the power transfer, allowing the system to operate at a fixed frequency [9], [18]. This method can also be used in output voltage regulation. Third, using a dc/dc converter in transmitting side or receiving side is also an effective way to regulate the final output voltage [6], [19]–[21]. In [20] and [21], the postregulation method is introduced to improve the so-called efficiency. However, the efficiency definition in [20] and [21] is based on the scattering matrix. It stands for the square of voltage gain rather than energy efficiency [14]. On the other hand, previous works that improve the system efficiency focus on resonant coil design [22], resonant topology selection [6], [23], and power amplifier optimization [24], [25].

As introduced earlier, the output voltage of a WPT system can be controlled by various methods. And the efficiency can also be improved from different aspects. Unfortunately, the reported output voltage regulation methods lack the consideration of achieving the highest efficiency. And the design approaches for high efficiency do not take account of the closed-loop characteristics. These studies rarely focus on both the output voltage regulation and the system efficiency maximization. It is only found in [26] that the higher side split frequency is carefully designed to achieve high efficiency and is tracked to maintain

Manuscript received January 16, 2014; revised April 25, 2014; accepted August 3, 2014. Date of publication August 19, 2014; date of current version February 13, 2015. This work was supported by the National Natural Science Foundation of China under Project 51177129. Recommended for publication by Associate Editor C. K. Tse.

The authors are with the School of Electrical Engineering, Xi'an Jiaotong University, Xi'an 710049, China (e-mail: hongchangli@stu.xjtu.edu.cn; lejie.china@qq.com; wangkangping@stu.xjtu.edu.cn; cwj@mail.xjtu.edu.cn; yangxu@mail.xjtu.edu.cn).

Color versions of one or more of the figures in this paper are available online at http://ieeexplore.ieee.org.

Digital Object Identifier 10.1109/TPEL.2014.2349534

constant output voltage. Nonetheless, tracking the split frequency cannot maintain an accurate constant output voltage when the equivalent series resistances (ESRs) of the coupled resonances are not zero, and the importance of using the optimum load resistance to achieve the highest efficiency is not noticed.

In this paper, an efficiency evaluation method is presented to evaluate four reported control schemes: lower side frequency control (LFC), higher side frequency control (HFC), preregulation, and postregulation. It shows that although the system's output voltage is maintained constant, the efficiency decreases after coupling or load varies. Furthermore, a maximum efficiency point tracking (MEPT) control scheme is proposed to maximize the system efficiency while regulating the output voltage. This control scheme fixes the operating frequency at the receiving-side resonant frequency to eliminate the power reflection. And it converts both the input voltage and the load resistance to maintain the operating point on the constant output voltage trajectory. In the meantime, the maximum efficiency point is dynamically tracked by matching the equivalent load resistance with its optimum value, which is related to the coupling coefficient.

The rest of this paper is organized as follows: Section II analyzes the output voltage and system efficiency of open-loop WPT systems. Section III presents the efficiency evaluation method for closed-loop WPT systems. In Section IV, the MEPT control scheme is proposed. The experiment is elaborated in Section V. Finally, the conclusion is shown in Section VI.

## II. Output Voltage and Efficiency of Open-Loop WPT Systems

### A. Circuit Model and Fundamental Harmonic Analysis (FHA)

In a WPT system using magnetic resonant coupling, power is transferred inductively by a pair of coupled coils. The coils' coupling coefficient $k$ is proportional to mutual inductance $M$

$$k = \frac{M}{\sqrt{L_1 L_2}} \tag{1}$$

where $L_1$ and $L_2$ are the inductances of the transmitting coil and the receiving coil, respectively.

To enhance the capacity of power transfer, improve the system efficiency, and lower the voltage and current stress of source and load, resonances need to be constructed in both the transmitting side and the receiving side. Four basic resonant topologies labeled as SS, SP, PS, and PP are shown in Fig. 1 [6], [7]. The capacitances $C_1$ and $C_2$ can be provided not only by external capacitors but also by the parasitic capacitances of the coils. The circuit can be driven either by ac voltage source or by ac current source according to the resonant type. The equivalent load resistance is $R_E$.

Among the four basic topologies, only the reactance of the SS topology looking from the power source is independent of either the coupling coefficient or the load resistance at the receiving-side resonant frequency

$$\omega_2 = \frac{1}{\sqrt{L_2 C_2}}. \tag{2}$$

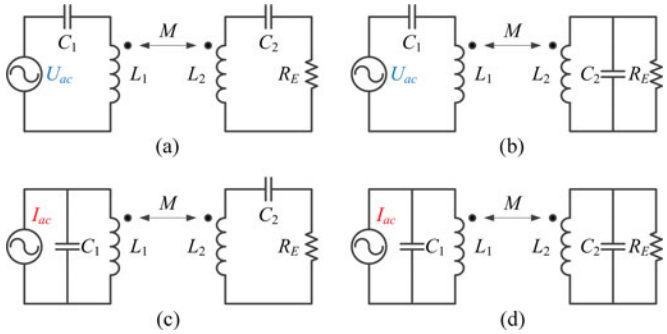


Fig. 1. Basic resonant topologies of WPT using magnetic resonant coupling: (a) SS, (b) SP, (c) PS, and (d) PP.

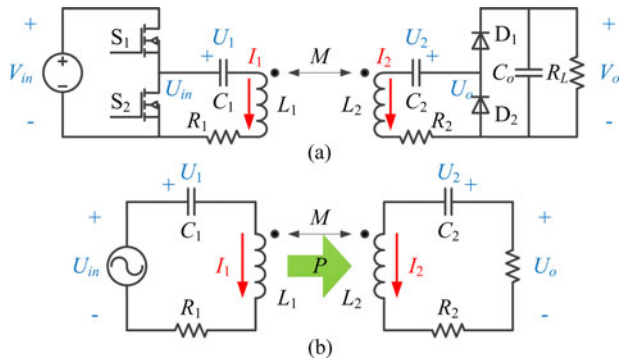


Fig. 2. (a) Half-bridge type WPT system using the SS topology, and (b) its fundamental harmonic equivalent circuit.

Furthermore, the power reflection from the receiving side to the transmitting side is eliminated at this frequency. Therefore, this paper selects the SS topology for the following discussion.

In most applications, a WPT system is fed by a dc voltage source and provides dc voltage to its load. In Fig. 2(a), the SS resonant tank is driven by a half-bridge inverter and the output voltage is rectified by a voltage-doubler rectifier. The dc input voltage is $V_{\text{in}}$ and the dc output voltage is $V_o$. The power losses of the WPT system, including conduction loss of the coils, radiation loss, conduction loss of the power semiconductors, and even switching loss, are related to the magnitudes of the resonant currents. Therefore, we use the ESRs $R_1$ and $R_2$ to stand for all the power losses. Definitely, the ESRs depend on operating point, i.e., operating frequency, resonant currents, etc. To simplify the analysis, we assume that the ESRs are constant.

Generally, the quality factors of the resonant tanks in a WPT system are very high. The resonant currents are almost sine waves. FHA based on the equivalent circuit in Fig. 2(b) has sufficient accuracy for the steady-state analysis. According to FHA, the system can be described by the following equations:

$$\begin{cases} \dot{U}_1 + j\omega_s L_1 \cdot \dot{I}_1 + j\omega_s M \cdot \dot{I}_2 + R_1 \dot{I}_1 = \dot{U}_{\text{in}} \\ \dot{U}_2 + j\omega_s L_2 \cdot \dot{I}_2 + j\omega_s M \cdot \dot{I}_1 + R_2 \dot{I}_2 = \dot{U}_o = -R_E \dot{I}_2 \\ j\omega_s C_1 \cdot \dot{U}_1 = \dot{I}_1 \\ j\omega_s C_2 \cdot \dot{U}_2 = \dot{I}_2 \end{cases} \tag{3}$$

TABLE I
SYSTEM PARAMETERS USED IN CALCULATION

| Symbol | Quantity | Value |
|---|---|---|
| $L_1, L_2$ | resonant inductances | 100 $\mu$H |
| $C_1, C_2$ | resonant capacitances | 1 nF |
| $R_1, R_2$ | ESRs | 1 $\Omega$ |
| $k$ | coupling coefficient | 0.05 |
| $R_L$ | load resistance | 78.2 $\Omega$ |
| $\omega_s$ | angular operating frequency | $3.16 \times 10^6$ rad/s |
| $f_s = \omega_s/2\pi$ | operating frequency | 503 kHz |

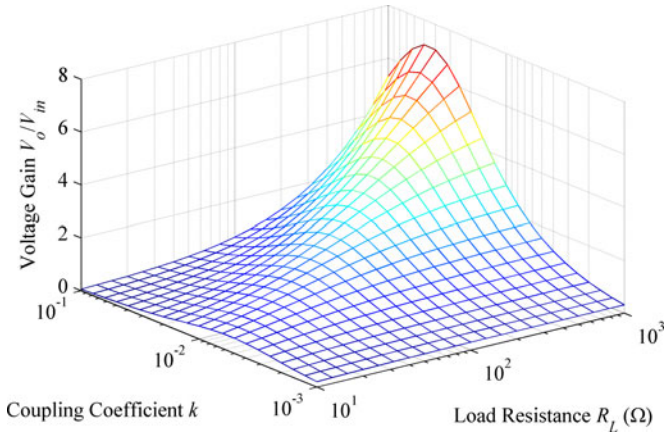


Fig. 3. Voltage gain as a function of coupling coefficient and load resistance.

where $\dot{U}_{\rm in}$ and $\dot{U}_o$ are the phasors of the fundamental harmonics of the ac input voltage and the ac output voltage, respectively; $\dot{U}_1$ and $\dot{U}_2$ are the phasors of the capacitors' voltages; $\dot{I}_1$ and $\dot{I}_2$ are the phasors of the inductors' currents; $\omega_s$ stands for the angular operating frequency; and $j$ is the imaginary unit. For the half-bridge type WPT system, the norms of $\dot{U}_{\rm in}$ and $\dot{U}_o$ can be calculated according to

$$U_{\rm in} = \left\|\dot{U}_{\rm in}\right\| = \frac{\sqrt{2}}{\pi} V_{\rm in} \tag{4}$$

$$U_o = \left\|\dot{U}_o\right\| = \frac{\sqrt{2}}{\pi} V_o. \tag{5}$$

The relationship between the equivalent load resistance $R_E$ and the system's load $R_L$ is

$$R_E = \frac{2}{\pi^2} R_L. \tag{6}$$

### B. Output Voltage

Substituting (4)–(6) into (3) with the parameters listed in Table I, the voltage gain $V_o/V_{\rm in}$ as a function of coupling coefficient and load resistance is calculated and plotted in Fig. 3. It shows that the voltage gain increases when the load resistance increases. For a fixed load resistance, there is a corresponding coupling coefficient that achieves the maximum voltage gain.

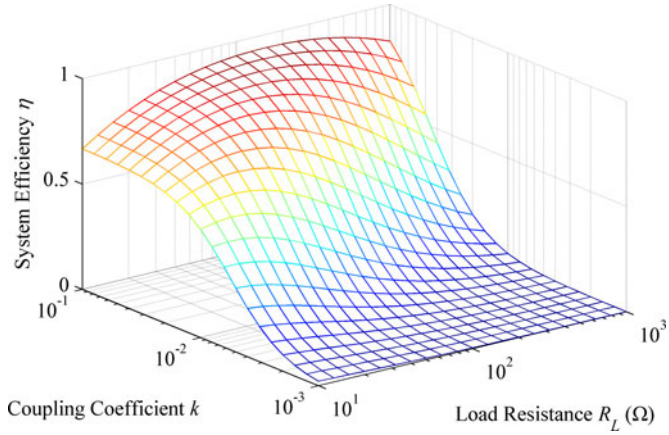


Fig. 4. System efficiency as a function of coupling coefficient and load resistance.

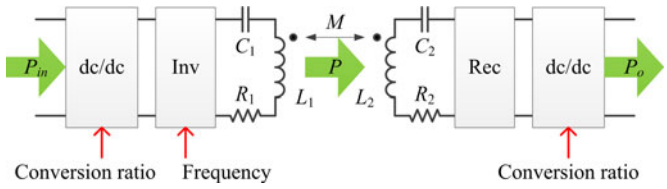


Fig. 5. Output voltage of a WPT system can be regulated using different control variables.

### C. System Efficiency

At the steady state, the system's efficiency is defined based on the input power and the output power

$$\eta = \frac{P_o}{P_{\rm in}} = \frac{V_o I_o}{V_{\rm in} I_{\rm in}} \tag{7}$$

where $I_{\rm in}$ is the dc input current and $I_o$ is the dc output current. Because all the power losses have been embodied in the ESRs, we can simply calculate the efficiency using the fundamental harmonic equivalent circuit. The result is given by

$$\eta = {\rm Re}\left[-\dot{U}_o \dot{I}_2^*\right] / {\rm Re}\left[\dot{U}_{\rm in} \dot{I}_1^*\right]. \tag{8}$$

Again, with the parameters listed in Table I, the system efficiency as a function of coupling coefficient and load resistance is calculated and plotted in Fig. 4. It shows that the efficiency drops when the coupling gets weaker. For a fixed coupling coefficient, there is a corresponding load resistance that achieves the maximum efficiency.

## III. CLOSED-LOOP WPT SYSTEMS AND THE EFFICIENCY EVALUATION METHOD

As a kind of power supply, WPT systems should first ensure the stable output voltage. When coupling coefficient or load resistance varies, a closed-loop WPT system can regulate the output voltage using different control variables as shown in Fig. 5. The system efficiency $P_o/P_{\rm in}$ of different control schemes is studied in this section.

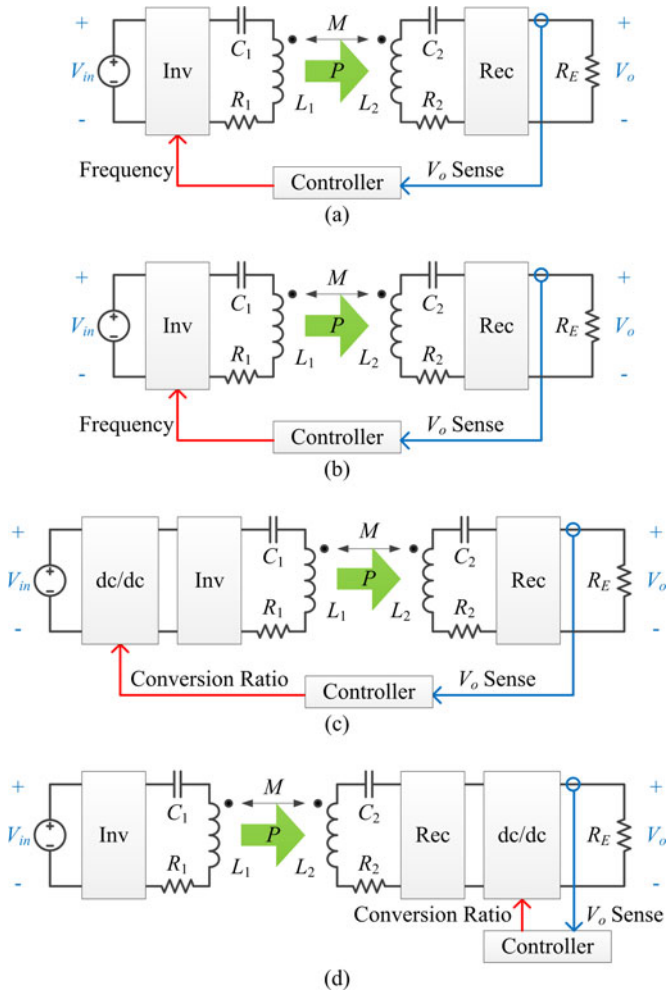


Fig. 6. Closed-loop control schemes maintaining constant output voltage. (a) LFC, (b) HFC, (c) preregulation, and (d) postregulation.

### A. Closed-Loop Control Schemes Maintaining Constant Output Voltage

Let us take four reported closed-loop control schemes: LFC, HFC, preregulation, and postregulation, as examples. The block diagrams of these control schemes are shown in Fig. 6.

*1) LFC:* It is shown in [9], [11], and [16] that the output voltage of an open-loop WPT system has two peaks near the split frequencies in the "over coupled" region. The output voltage increases when the operating frequency changes from zero to $\omega_{Lpk}$ at which the first peak occurs. Based on this, LFC controls the output voltage by adjusting the operating frequency.

*2) HFC:* Oppositely, HFC adjusts the operating frequency from $\omega_{Hpk}$ at which the second peak occurs to infinite (theoretically). The output voltage decreases when the operating frequency increases. The hardware and algorithm of LFC and HFC are almost the same. They are, respectively, selected to achieve zero-current switching and zero-voltage switching (ZVS) in the inverter.

*3) Preregulation:* Without changing the operating frequency, the system's output voltage can be linearly regulated using a dc/dc converter in the transmitting side. The input voltage conversion ratio

$$C_{\text{Input}} = V_{\text{o\_converter}}/V_{\text{in}} \tag{9}$$

is considered as the control variable, where $V_{\text{o\_converter}}$ is the output voltage of the dc/dc converter. The voltage gain of the system is the product of the voltage gain of the dc/dc converter and the voltage gain from the inverter's input to the rectifier's output.

*4) Postregulation:* Alternatively, we can put the dc/dc converter in the receiving side to regulate the output voltage. The load conversion ratio

$$C_{\text{load}} = R_{\text{in\_converter}}/R_L \tag{10}$$

is considered as the control variable, where $R_{\text{in\_converter}}$ is the equivalent input resistance of the dc/dc converter. Comparing with the preregulation, the voltage gain from the inverter's input to the rectifier's output is related to the load conversion ratio, because the equivalent load resistance $R_E$ is converted by the dc/dc converter in the receiving side.

Using the parameters listed in Table I and the FHA method demonstrated in Section II, the system's voltage gain $V_o/V_{\text{in}}$ and efficiency are calculated versus the control variables. Fig. 7 shows the results of the four control schemes. It should be illustrated that the dc/dc converters used in the preregulation and the postregulation are assumed to be lossless.

### B. Efficiency Evaluation Method

Once the output voltage is maintained constant by a closed-loop control system, the relationship between the coupling coefficient/load resistance and efficiency will be quite different from that is shown in Fig. 4. Based on the circuit model in Fig. 6, the efficiency evaluation method investigates the closed-loop system's efficiency at various coupling and load conditions, while the input voltage is fixed and the output voltage is maintained constant.

In the first step, the input voltage of the open-loop WPT system (with the parameters listed in Table I) is fixed at 100 V. Its output voltage is calculated to be 93.9 V. In the second step, we change the coupling coefficient and the load resistance. To maintain the output voltage constant (93.9 V), the control variable of the closed-loop system has to be adjusted. For example, the operating frequency to achieve 93.9 V output voltage is numerically solved for the changed coupling and load condition when LFC is used. In the last step, the efficiency of the system at the new operating point is calculated using the FHA method.

The calculation results of the four control schemes are shown in Fig. 8. The closed-loop system efficiency always drops sharply when the coupling gets weaker, and the load variation also causes a significant efficiency decrease. It is worth mentioning that some control schemes have no solution to achieve the constant output voltage when the coupling is too strong or the load resistance is too small. This can be explained by the control curves plotted in Fig. 7.

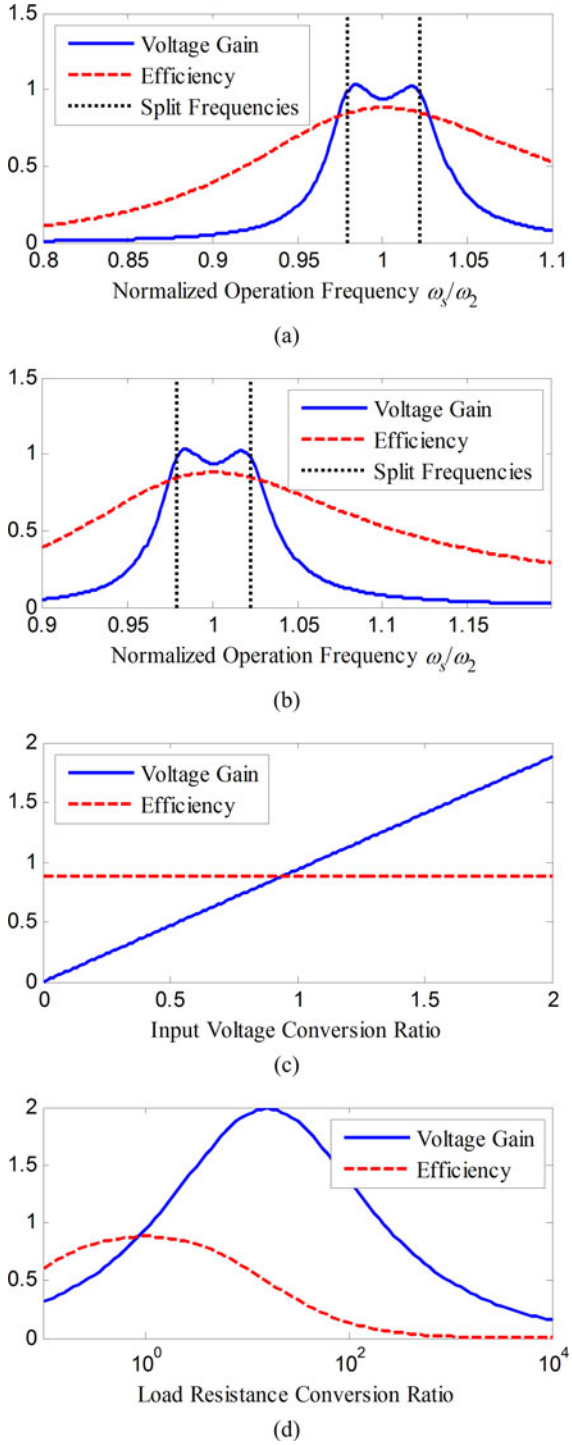


Fig. 7. Voltage gain and system efficiency of (a) LFC, (b) HFC, (c) preregulation, and (d) postregulation versus control variables.

## IV. MEPT Control Scheme

As is demonstrated in Section III, more than one control variable can be used to regulate the output voltage. A control scheme that adjusts two independent variables may have a chance to maintain the constant output voltage and maximize the efficiency at the same time. The MEPT control scheme is proposed based upon this point.

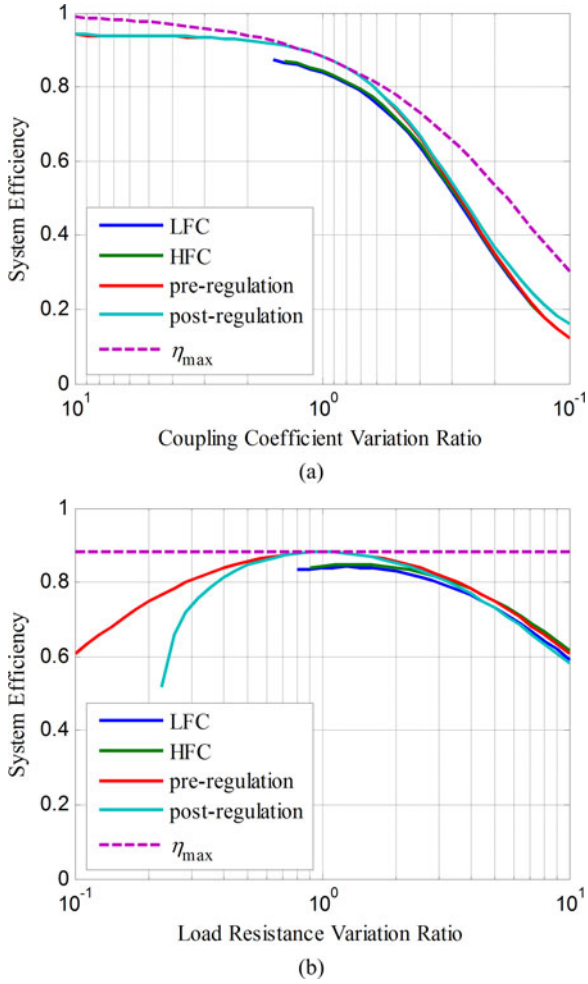


Fig. 8. Closed-loop system efficiency of different control schemes (a) with coupling variation and fixed load resistance $R_L = 78.2\,\Omega$, and (b) with load variation and fixed coupling coefficient $k = 0.05$.

### A. Maximum Efficiency Point

The maximum efficiency point is such an operating point that the operating frequency equals the receiving-side resonant frequency

$$\omega_s = \omega_2 \tag{11}$$

to eliminate the power reflection, and the equivalent load resistance matches its optimum value [12], [27]

$$R_E = R_{E\_op} = \sqrt{1 + fom^2} \cdot R_2 \tag{12}$$

to minimize the ESR losses, where the figure-of-merit is related to the mutual inductance (as well as the coupling coefficient)

$$fom = \frac{\omega_s M}{\sqrt{R_1 R_2}}. \tag{13}$$

Therefore, the optimum equivalent load resistance is related to coupling coefficient. When both (11) and (12) are satisfied, the maximum efficiency is given by (14) as derived in [27]. It is plotted using the dashed line in Fig. 8 with the parameters in

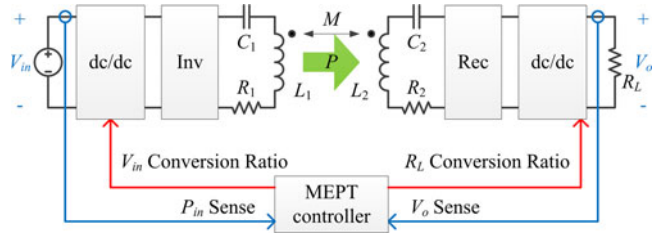


Fig. 9. Closed-loop system structure of the MEPT control scheme.

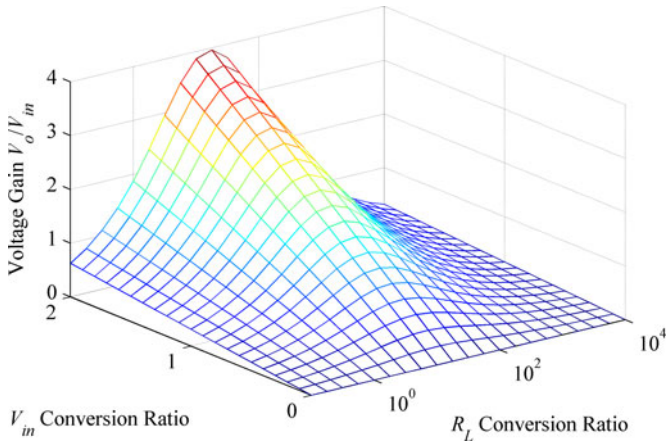


Fig. 10. System's voltage gain as a function of input voltage conversion ratio and load resistance conversion ratio.

Table I

$$\eta_{\max} = 1 - \frac{2}{\sqrt{1 + fom^2} + 1}. \tag{14}$$

### B. Principle of MEPT

There is an important assumption in the analysis of the maximum efficiency point: the WPT system only has the ESR losses. In Section II-A, the power losses in the inverter and the rectifier have been converted into the ESR losses. And for a WPT system, the power loss of the power stage from the inverter's input to the rectifier's output is usually the major loss. Therefore, the principle of MEPT is based on (11)–(14).

The MEPT control scheme fixes the operating frequency at the receiving-side resonant frequency to satisfy (11). It converts the load resistance by a dc/dc converter to match the equivalent load resistance with its optimum value in (12). At the same time, the input voltage is regulated by another dc/dc converter in the transmitting side to regulate the system's output voltage. Therefore, the MEPT control scheme uses two control variables: the input voltage conversion ratio and the load resistance conversion ratio. Fig. 9 shows its closed-loop system structure.

To provide a visual illustration, Fig. 10 shows the 3-D plot of the voltage gain $V_o/V_{\text{in}}$ as a function of the input voltage conversion ratio and the load resistance conversion ratio (according to the parameters listed in Table I).

Fig. 11 shows a schematic plot of a contour line on the mountain in Fig. 10. The contour line is a constant output voltage trajectory. The MEPT control scheme restricts the operating point on the constant output voltage trajectory when coupling or load varies. And it moves the operating point along the trajectory to find the maximum efficiency point, at which the equivalent load resistance matches its optimum value.

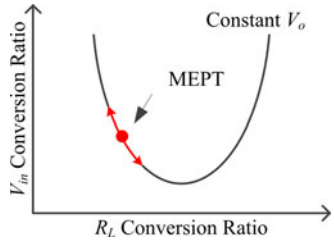


Fig. 11. MEPT on a constant output voltage trajectory (schematic plot).

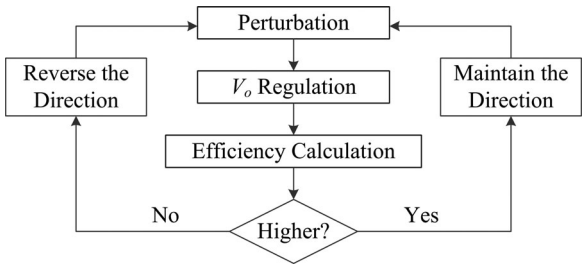


Fig. 12. Flowchart of the MEPT control scheme.

Although we can calculate the optimum equivalent load resistance according to (12), the mutual inductance depends on the placement and the ESRs are not actually constant (depending on the operating point). As a consequence, the maximum efficiency point cannot be predicted exactly. We have to track it in real time using the MEPT method.

### C. Realization Method

In the system shown in Fig. 9, one of the two dc/dc converters is used to regulate the output voltage and the other one is used to perturb the operating point by changing its conversion ratio. The controller records the efficiency for each step of the perturbation and reregulation. The direction of perturbation is maintained for the next step if the efficiency gets higher; otherwise, it is reversed. Fig. 12 shows this flowchart.

In addition, there are two tips that simplify the system and promote the performance. The first one is tracking the minimum dc input current instead of the maximum efficiency. Actually, the minimum input current is an equivalent condition of the maximum efficiency when the input voltage is fixed and the output voltage is maintained constant. The second one is regulating the output voltage by the receiving-side dc/dc converter and perturbing the operating point by the transmitting-side dc/dc converter. With this method, the voltage regulation loop does not involve the wireless communication link between the two sides and both the speed and the stability can be improved.

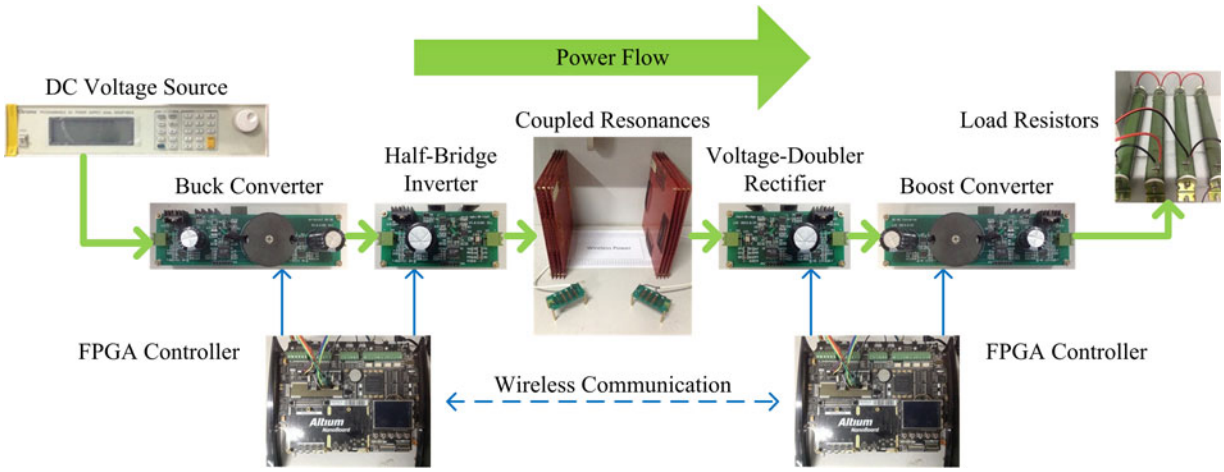


Fig. 13. Experimental setup of the WPT system.

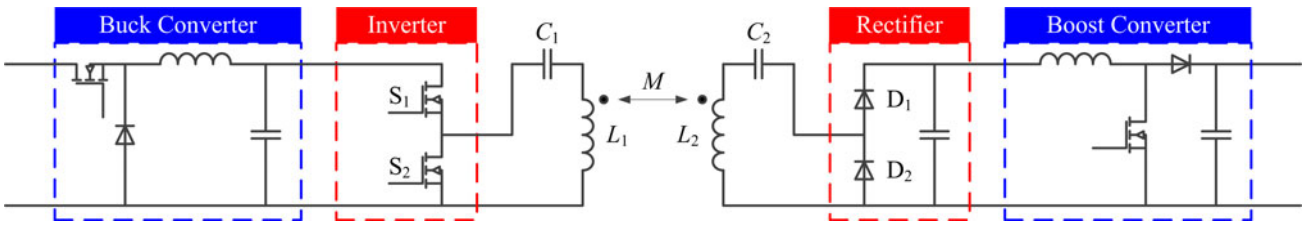


Fig. 14. Circuit diagram of the power stages.

TABLE II
PARAMETERS OF THE EXPERIMENTAL SYSTEM

| Symbol | Quantity | Value |
|---|---|---|
| $L_1$ | transmitting-side inductance | 131 $\mu$H |
| $C_1$ | transmitting-side capacitance | 0.75 nF |
| $R_{\mathrm{ac1}}$ | ac resistance of transmitting coil | 0.71 $\Omega$ |
| $R_{\mathrm{ds\_on}}$ | on-time drain-to-source resistance of $S_1$ and $S_2$ | 0.66 $\Omega$ |
| $\omega_1$ | angular resonant frequency of transmitting-side resonator | $3.19 \times 10^6$ rad/s |
| $L_2$ | receiving-side inductance | 127 $\mu$H |
| $C_2$ | receiving-side capacitance | 0.75 nF |
| $R_{\mathrm{ac2}}$ | ac resistance of receiving coil | 0.57 $\Omega$ |
| $V_f$ | forward voltage of $D_1$ and $D_2$ | 1.0 V at 1 A |
| $\omega_2$ | angular resonant frequency of receiving-side resonator | $3.24 \times 10^6$ rad/srad/s |
| $f_s$ | operating frequency | 515 kHz |

## V. EXPERIMENT

### A. Experimental System

Fig. 13 shows the experimental setup of the WPT system. The circuit diagram of the power stages is shown in Fig. 14. Starting from a dc voltage source, the power flows through a buck converter, a half-bridge inverter, a pair of magnetically coupled resonances, a voltage-doubler rectifier, and a boost converter. Finally, it is provided to load resistors. The buck converter and the boost converter are controlled by the pulse-width-modulation signals (100 kHz) from two field-programmable gate array (FPGA) controllers, respectively (Altium NanoBoard 3000 with Altera Cyclone III). The metal–oxide–semiconductor field-effect transistors (MOSFETs) in the half-bridge inverter are controlled by a pair of complementary drive signals (515 kHz) generated by the transmitting-side FPGA controller. The two FPGA controllers exchange signals and instructions by 2.4 GHz wireless communication modules. Parameters of the system are listed in Table II.

Both the coupled coils are made by Litz wire. The structure of the windings is carefully designed to lower the ac resistance and to increase the coupling coefficient. The diameter of the outer loop is 27 cm and the thickness is about 3 cm (as shown in Fig. 15). The coupling coefficient of the two coils at different face-to-face distances is simulated using Ansoft Maxwell 13. The result is shown in Fig. 16.

The inductance of the transmitting coil is intentionally designed to be a little larger than the inductance of the receiving

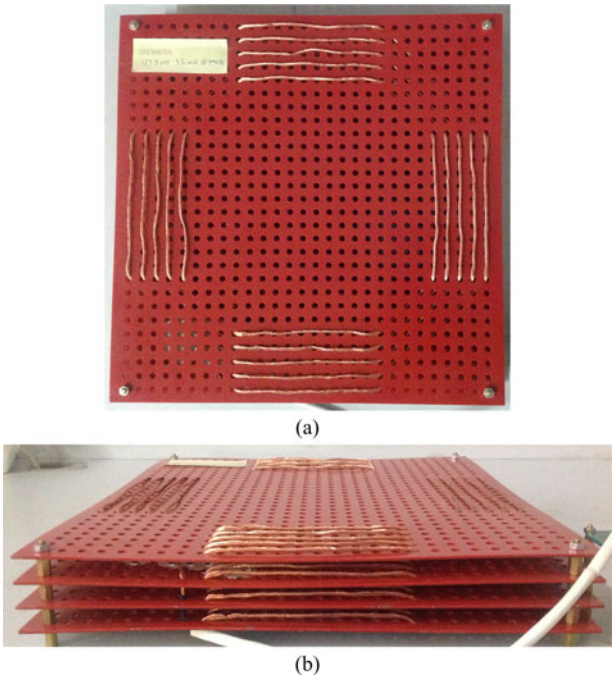


Fig. 15. The multilayer spiral coil with 27 cm outer-loop diameter and 3 cm thickness: (a) front view and (b) side view.

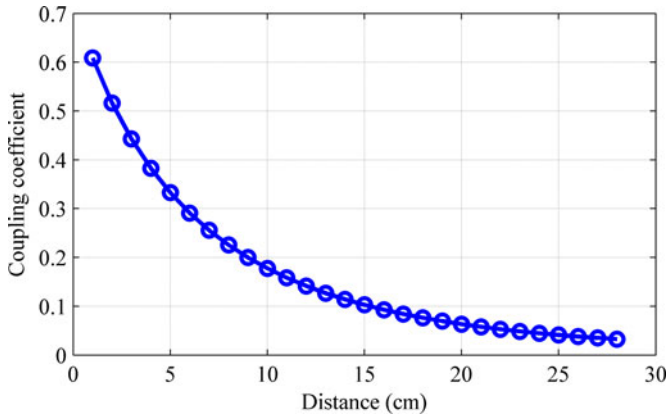


Fig. 16. Coupling coefficient versus face-to-face distance (simulation result).

coil to lower the transmitting-side resonant frequency. Therefore, the inverter has an inductive load to achieve ZVS when it operates at the receiving-side resonant frequency [27]. The cost is the reduction of the system's voltage gain.

### B. Open-Loop Operation Test

We first test the experimental system in open loop. Both the buck converter and the boost converter are removed from the power flow path. The rest circuit is as shown in Fig. 2. The input voltage is set to 125 V and the load resistance is manually optimized to be 120 Ω. Under these conditions, 100 W power is transferred to the load across 20 cm.

The open-loop operating waveforms are shown in Fig. 17. The drain-to-source voltage $V_{\rm ds}$ of $S_2$ drops to zero before

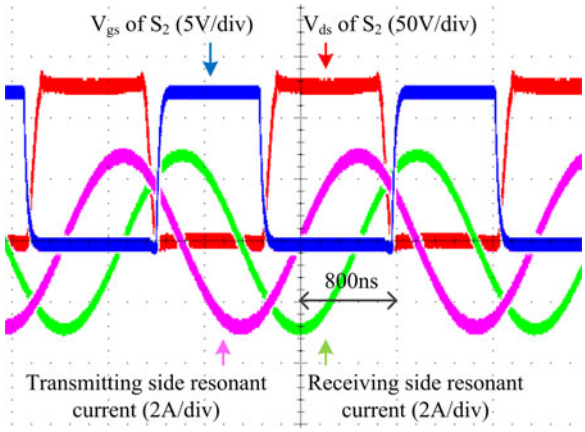


Fig. 17. Open-loop operating waveforms.

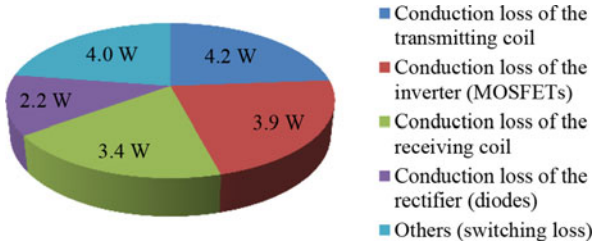


Fig. 18. Loss breakdown of the open-loop operation.

the gate drive voltage $V_{\rm gs}$ of $S_2$ gets to high level. It proves the ZVS is achieved. The phase difference between the two resonant currents is about 90°. It indicates the operating frequency equals the receiving-side resonant frequency and there is no power reflection.

The input voltage $V_{\rm in}$ and current $I_{\rm in}$ of the system are measured by the power source (5.5 digit). The output voltage $V_o$ and current $I_o$ are measured by multimeters (4.5 digit) with a 100 mΩ current shunt resistor (1% precision). The overall efficiency is calculated to be 85% according to (7) and the power loss is about 17.7 W. In Fig. 18, we break down the power loss using the parameters listed in Table II and the measured resonant currents (the peak values are about 2.7 A).

### C. Validation of the MEPT Control Scheme

In the open-loop operation test, the power transfer distance is fixed at 20 cm and the load resistance is carefully adjusted to achieve a high efficiency. To validate the MEPT control scheme, we test the closed-loop system in different coupling and load conditions. The input voltage of the system is fixed at 200 V. The output voltage is always regulated to 100 V by the three control schemes: HFC, preregulation, and MEPT respectively. The other two control schemes: LFC and postregulation are not involved because they violate the ZVS operation principle in some coupling and load conditions. The switching loss increases significantly and even damages the MOSFETs without ZVS.

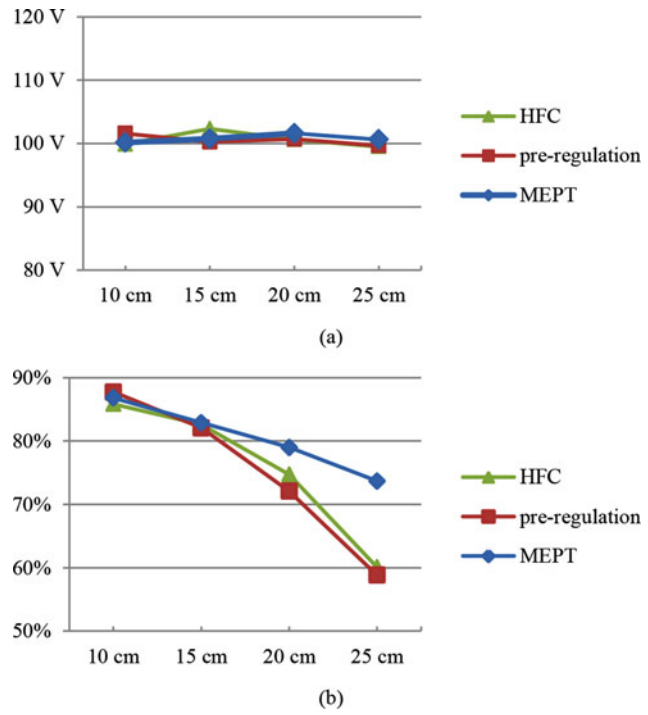


Fig. 19. Closed-loop system test with 400 Ω load resistance at different power transfer distances: (a) output voltage and (b) overall efficiency.

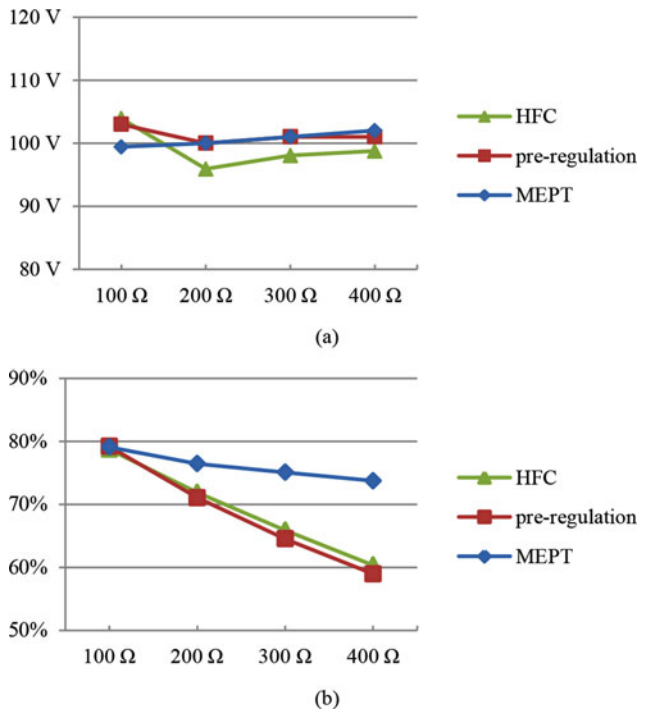


Fig. 20. Closed-loop system test at 25 cm power transfer distance with different load resistances: (a) output voltage and (b) overall efficiency.

In the first closed-loop test, we use 400 Ω load resistance and change the power transfer distance from 10 to 25 cm. The output voltage and the overall efficiency are measured and shown in Fig. 19. In the second closed-loop test, we fix the power transfer distance at 25 cm and change the load resistance from 100 to 400 Ω. The output voltage and the overall efficiency are measured and shown in Fig. 20. Although the control accuracy of the output voltage is limited by the sensors and the resolution of the digital system, the accuracy of the efficiency that is calculated according to the measured voltages and currents is believed to be 1%.

Comparing with the result of the open-loop test (85% efficiency with the optimized load resistance at 20 cm), the efficiency of the MEPT control scheme at 20 cm is only 79%. There is 6% power loss on the dc/dc converters. However, the boost converter in the receiving side is removed when implementing preregulation. Both the two dc/dc converters are removed when implementing HFC. Even though the dc/dc converters produce some additional power loss, the closed-loop system with MEPT control scheme achieves a much higher overall efficiency over wide ranges of coupling coefficient and load resistance. This is because only the MEPT control scheme matches the equivalent load resistance with its optimum value corresponded to the coupling coefficient.

According to the circuit model in Fig. 2, we can estimate the ESR of the transmitting side using the sum of the ac resistance $R_{\mathrm{ac1}}$ of the transmitting coil and the on-time drain-to-source resistance $R_{\mathrm{ds\_on}}$ of the MOSFETs

$$R_1 \approx R_{\mathrm{ac1}} + R_{\mathrm{ds\_on}}. \tag{15}$$

The minor switching loss is neglected. Similarly, the ESR of the receiving side is estimated by

$$R_2 \approx R_{\mathrm{ac2}} + \frac{2V_f I_f}{I_2^2} \tag{16}$$

where $R_{\mathrm{ac2}}$ is the ac resistance of the receiving coil, $V_f$ is the forward voltage of the rectifier diode, $I_f$ is the average forward current of each diode, and $I_2$ is the RMS value of the receiving-side resonant current.

For each operating point, the optimum equivalent load resistance $R_E$ can be derived out by substituting (15) and (16), the operating frequency, the inductances in Table II, and the simulated coupling coefficient in Fig. 16 into (13) and (12). The results are shown in Fig. 21. The optimum equivalent load resistance decreases when the power transfer distance increases because the figure-of-merit in (13) decreases. The system's load $R_L$ also has a little influence on the optimum equivalent load resistance because the average forward current $I_f$ and the ESR $R_2$ are not constant for different $R_L$.

In the experiment, the MEPT control scheme finds the optimum equivalent load resistance by tracking algorithm. It converts the load resistance by adjusting the duty ratio $D$ of the boost converter. The converted equivalent load resistance

$$R_E = \frac{2}{\pi^2}(1-D)^2 R_L \tag{17}$$

is plotted in Fig. 21 using the experimental data records. In contrast, the equivalent load resistance without conversion (duty ratio $D = 0$) is also shown. In Fig. 21(a), the MEPT control scheme converts the 400 Ω load resistance to match it with the different optimum equivalent load resistances corresponded

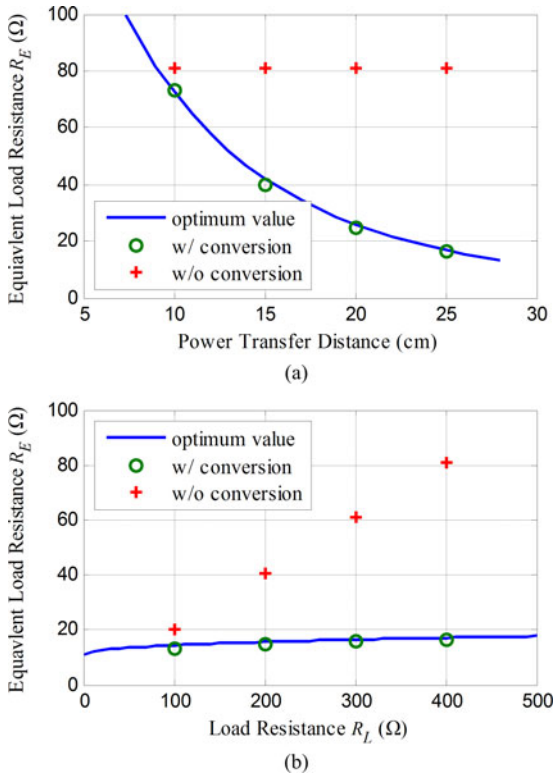


Fig. 21. Comparison of the estimated optimum equivalent load resistance, converted equivalent load resistance, and the equivalent load resistance without conversion: (a) under different coupling conditions and (b) under different load conditions.

to power transfer distance. Similarly, in Fig. 21(b), the MEPT control scheme converts the different load resistances to match the optimum equivalent load resistance at 25 cm. Therefore, the MEPT control scheme has higher efficiency than the other control schemes as shown in Figs. 19 and 20. The maximum efficiency point analysis is validated by Fig. 21. However, the efficiency that is calculated using (15) and (16) is higher than the measured overall efficiency. The reason is that the switching loss and the losses in the dc/dc converters are not taken into account in the calculation.

## VI. Conclusion

By analyzing the output voltage and system efficiency of the open-loop WPT system, this paper illustrates the necessity of the closed-loop control against coupling and load variations. An efficiency evaluation method is presented to evaluate the four typical closed-loop control schemes: LFC, HFC, preregulation, and postregulation. Although the output voltage can be maintained constant with these schemes, the system's efficiency drops significantly when coupling or load varies. Based upon these analysis results, a MEPT control scheme is proposed to maximize the system efficiency while regulating the output voltage. Both the maximum efficiency point and the principle of MEPT as well as the realization method are elaborated. In experiment, the MEPT control scheme is compared with HFC and preregulation. Although the closed-loop system that uses MEPT control scheme has more power loss on the additional dc/dc converters, it achieves a much higher overall efficiency over wide ranges of coupling coefficient and load resistance. The MEPT control scheme is more effective in two cases: one is that the power transfer distance is relatively long (weak coupling), and the other one is that the equivalent load resistance is far away from its optimum value.

## References

[1] N. Tesla, "Apparatus for transmitting electrical energy," U.S. Patent 1 119 732, 1914.
[2] A. S. Marincic, "Nikola Tesla and the wireless transmission of energy," *IEEE Trans. Power App. Syst.*, vol. PAS-101, no. 10, pp. 4064–4068, Oct. 1982.
[3] J. Garnica, R. A. Chinga, and J. Lin, "Wireless power transmission: From far field to near field," *Proc. IEEE*, vol. 101, no. 6, pp. 1321–1331, Jun. 2013.
[4] S. Y. Hui, "Planar wireless charging technology for portable electronic products and Qi," *Proc. IEEE*, vol. 101, no. 6, pp. 1290–1301, Jun. 2013.
[5] Y. Hori, "Novel EV society based on motor/capacitor/wireless," in *Proc. IEEE MTT-S Int. Microw. Workshop Series Innovative Wireless Power Transmiss.: Technol. Syst. Appl.*, May 2012, pp. 3–8.
[6] C. Wang, O. H. Stielau, and G. A. Covic, "Design considerations for a contactless electric vehicle battery charger," *IEEE Trans. Ind. Electron.*, vol. 52, no. 5, pp. 1308–1314, Oct. 2005.
[7] J. Sallán, J. L. Villa, A. Llombart, and J. F. Sanz, "Optimum design of ICPT systems applied to electric vehicle battery charge," *IEEE Trans. Ind. Electron.*, vol. 56, no. 6, pp. 2140–2149, Jun. 2009.
[8] P. Si, A. P. Hu, S. Malpas, and D. Budgett, "A frequency control method for regulating wireless power to implantable devices," *IEEE Trans. Biomed. Circuits Syst.*, vol. 2, no. 1, pp. 22–29, Mar. 2008.
[9] B. H. Waters, A. P. Sample, P. Bonde, and J. R. Smith, "Powering a ventricular assist device (VAD) with the free-range resonant electrical energy delivery (FREE-D) system," *Proc. IEEE*, vol. 100, no. 1, pp. 138–149, Jan. 2012.
[10] R. Xue, K. Cheng, and M. Je, "High-efficiency wireless power transfer for biomedical implants by optimum resonant load transformation," *IEEE Trans. Circuits Syst.-I, Reg. Papers*, vol. 60, no. 4, pp. 867–874, Apr. 2013.
[11] D. Ahn and S. Hong, "Wireless power transmission with self-regulated output voltage for biomedical implant," *IEEE Trans. Ind. Electron.*, vol. 61, no. 5, pp. 2225–2235, May 2014.
[12] A. Kurs, A. Karalis, R. Moffatt, J. D. Joannopoulos, P. Fisher, and M. Soljačić, "Wireless power transfer via strongly coupled magnetic resonances," *Science*, vol. 317, no. 5834, pp. 83–86, Jul. 2007.
[13] C. Chen, T. Chu, C. Lin, and Z. Jou, "A study of loosely coupled coils for wireless power transfer," *IEEE Trans. Circuits Syst.-II, Exp. Briefs*, vol. 57, no. 7, pp. 536–540, Jul. 2010.
[14] S. Y. R. Hui, W. X. Zhong, and C. K. Lee, "A critical review of recent progress in mid-range wireless power transfer," *IEEE Trans. Power Electron.*, vol. 29, no. 9, pp. 4500–4511, Sep. 2014.
[15] Z. N. Low, R. A. Chinga, R. Tseng, and J. Lin, "Design and test of a high-power high-efficiency loosely coupled planar wireless power transfer system," *IEEE Trans. Ind. Electron.*, vol. 56, no. 5, pp. 1801–1812, May 2009.
[16] A. P. Sample, D. A. Meyer, and J. R. Smith, "Analysis, experimental results, and range adaptation of magnetically coupled resonators for wireless power transfer," *IEEE Trans. Ind. Electron.*, vol. 58, no. 2, pp. 544–554, Feb. 2011.
[17] N. Y. Kim, K. Y. Kim, J. Choi, and C. W. Kim, "Adaptive frequency with power-level tracking system for efficient magnetic resonance wireless power transfer," *Electron. Lett.*, vol. 48, no. 8, pp. 452–454, Apr. 2012.
[18] T. C. Beh, M. Kato, T. Imura, S. Oh, and Y. Hori, "Automated impedance matching system for robust wireless power transfer via magnetic resonance coupling," *IEEE Trans. Ind. Electron.*, vol. 60, no. 9, pp. 3689–3698, Sep. 2013.
[19] J. Yin, D. Lin, C. K. Lee, and S. Y. Hui, "Load monitoring and output power control of a wireless power transfer system without any wireless communication feedback," in *Proc. IEEE Energy Convers. Congr. Expo.*, Sep. 2013, pp. 4934–4939.
[20] Y. Moriwaki, T. Imura, and Y. Hori, "Basic study on reduction of reflected power using dc/dc converters in wireless power transfer system via

magnetic resonant coupling," in *Proc. IEEE 33rd Int. Telecommun. Energy Conf.*, Oct. 2011, pp. 1–5.
[21] M. Fu, C. Ma, and X. Zhu, "A cascaded boost-buck converter for high efficiency wireless power transfer systems," *IEEE Trans. Ind. Informat.*, vol. 10, no. 3, pp. 1972–1980, Aug. 2014.
[22] S. H. Lee and R. D. Lorenz, "Development and validation of model for 95% efficiency 220W wireless power transfer over a 30cm air-gap," *IEEE Trans. Ind. Appl.*, vol. 47, no. 6, pp. 2495–2504, Nov. 2011.
[23] L. Chen, S. Liu, Y. C. Zhou, and T. J. Cui, "An optimizable circuit structure for high-efficiency wireless power transfer," *IEEE Trans. Ind. Electron.*, vol. 60, no. 1, pp. 339–349, Jan. 2011.
[24] J. J. Casanova, Z. N. Low, and J. Lin, "Design and optimization of a class-E amplifier for a loosely coupled planar wireless power system," *IEEE Trans. Circuits Syst.-II, Exp. Briefs*, vol. 56, no. 11, pp. 830–834, Nov. 2009.
[25] M. Pinuela, D. C. Yates, S. Lucyszyn, and P. D. Mitcheson, "Maximizing dc-to-load efficiency for inductive power transfer," *IEEE Trans. Power Electron.*, vol. 28, no. 5, pp. 2437–2447, May 2013.
[26] W. Zhang, S. C. Wong, C. K. Tse, and Q. Chen, "Design for efficiency optimization and voltage controllability of series-series compensated inductive power transfer systems," *IEEE Trans. Power Electron.*, vol. 29, no. 1, pp. 191–200, Jan. 2014.
[27] H. Li, X. Yang, K. Wang, and X. Dong, "Study on efficiency maximization design principles for wireless power transfer system using magnetic resonant coupling," in *Proc. Energy Convers. Congr. Expo. Asia*, Jun. 2013, pp. 888–892.

**Hongchang Li** (S'12) was born in Luoyang, China, in 1991. He received the B.S. degree in electrical engineering from Xi'an Jiaotong University, Xi'an, China, in 2011, where he is currently working toward the Ph.D. degree in electrical engineering.

His current research interests include wireless power transfer and digital control techniques.

**Jie Li** received the B.S. degree in electrical engineering from Xi'an Jiaotong University, Xi'an, China, in 2014.

His current research interests include power electronics application on wireless energy transmission and system control.

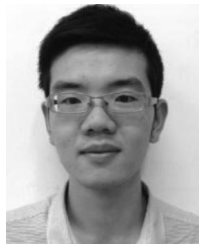

**Kangping Wang** (S'14) was born in Shaanxi, China, in 1989. He received the B.S. degree in electrical engineering from Xi'an Jiaotong University, Xi'an, China, in 2012, where he is currently working toward the Ph.D. degree in electrical engineering.

His current research interests include power electronic integration and packaging technologies.

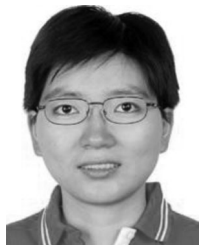

**Wenjie Chen** (S'06–M'08) received the B.S., M.S., and Ph.D. degrees in electrical engineering from Xi'an Jiaotong University, Xi'an, China, in 1996, 2002, and 2006, respectively.

Since 2002, she has been a member of the faculty of School of Electrical Engineering, Xi'an Jiaotong University, where she is currently a Professor. From January 2012 to January 2013, she was with the Department of Electrical Engineering and Computer Science, University of Tennessee, Knoxville, TN, as a Visiting Scholar. She then came back to Xi'an Jiaotong University, and was involved in the teaching and researches in power electronics. Her main research interests include electromagnetic interference, active filters, and power electronic integration.

**Xu Yang** (M'02) received the B.S. and Ph.D. degrees in electrical engineering from Xi'an Jiaotong University, Xi'an, China, in 1994 and 1999, respectively.

Since 1999, he has been a member of the faculty of School of Electrical Engineering, Xi'an Jiaotong University, where he is currently a Professor. From November 2004 to November 2005, he was with the Center of Power Electronics Systems, Virginia Polytechnic Institute and State University, Blacksburg, VA, as a Visiting Scholar. He then came back to Xi'an Jiaotong University, and was involved in the teaching and researches in power electronics and industrial automation area. His research interests include soft-switching topologies, pulse width modulation control techniques and power electronic integration, and packaging technologies.